Tailored photon-pair sources based on inner-loop phasematching in fiber-based spontaneous four-wave mixing

K. Garay-Palmett[a], A.B. U'Ren[a], and R. Rangel-Rojo[b]
[a]*Instituto de Ciencias Nucleares, Universidad Nacional Autónoma de México, Apartado Postal 70-543, México, DF, 04510, México.*
[b]*Departamento de Óptica, Centro de Investigación Científica y de Educación Superior de Ensenada, Apartado Postal 2732, Ensenada, BC 22860, México.*

Recibido el 25 de enero de 2011; aceptado el 31 de marzo de 2011

We study the generation of photon pairs by spontaneous four-wave mixing (SFWM) in photonic crystal optical fibers. We show that it is possible to engineer two-photon states with specific spectral entanglement properties suitable for quantum information processing applications. In this work, we concentrate on inner-loop phasematching, for which signal and idler photons can be generated at a small spectral separation from the pump, while sufficiently removed from the pump to ensure the absence of background photons produced by spontaneous Raman scattering. We present specific source designs which permit both symmetric and asymmetric factorable states, which allow heralding of pure-state, single-photon wavepackets without the need for spectral post-filtering. Additionally, we present numerical results for the conversion efficiency, where we compare sources based on inner- and outer-loop phasematching.

Keywords: Photonic nonclassical states; quantum entanglement; four-wave mixing

Estudiamos la generación de parejas de fotones por mezclado de cuatro ondas espontáneo (SFWM) en fibras de cristal fotónico. Mostramos que es posible acondicionar el estado de dos fotones, de manera que exhiba propiedades de correlación espectral específicas, convenientes para aplicaciones en procesamiento de información cuántica. En este trabajo, nos concentramos en parejas que yacen en el loop interior de la curva de empatamiento de fases, para el cual los fotones señal y acompañante pueden ser generados a una desintonización pequeña con respecto a la frecuencia de bombeo, pero lo suficientemente alejadas de ésta para garantizar la supresión de fotones producidos por esparcimiento Raman espontáneo. Presentamos diseños de fuentes específicas, que favorecen la generación de estados factorizables simétricos y asimétricos, los cuales permiten la anunciación de paquetes de ondas unifotónicos en estado puro sin la necesidad de filtrado espectral posterior. Adicionalmente, mostramos resultados numéricos de la eficiencia de conversión SFWM obtenida en las ramas interiores y exteriores del contorno de empatamiento de fases.

Descriptores: Estados fotónicos no clásicos; entrelazamiento cuántico; mezclado de cuatro ondas

PACS: 42.50.-p, 03.65.Ud, 42.65.-k, 42.65.Hw

1. Introduction

Quantum optical technologies require photon states with specific spectral properties. For example, pure-state single heralded photon generation, of key importance for quantum networking, requires factorable two-photon states, *i.e.* without correlations, when considering all photonic degrees of freedom [1]. Typically, however, photon pairs generated by spontaneous parametric nonlinear optical processes exhibit significant spectral and spatial correlations due to the energy and momentum conservation constraints. Spatial correlations may be minimized by the use of guided-wave configurations, such as those exploiting nonlinear waveguides and optical fibers [2-4]. It has been shown that it is possible to eliminate spectral correlations for photon pairs generated by means of spontaneous parametric downconversion (SPDC) [5,6], and recently by means of SFWM in photonic crystal fibers (PCFs) [7-10], through group-velocity matching techniques, together with the use of broadband pulsed pumps.

In Ref. 7 it has been shown that the SFWM process in PCF permits the emission of photon pairs with spectrally engineered properties with considerably greater flexibility than for the case of SPDC in second-order nonlinear crystals. Thus, for example, we have shown that for a given fiber exhibiting two zero-dispersion frequencies within the spectral window of interest, it is possible to obtain states with an arbitrary degree of spectral entanglement, controlled by the pump frequency. Nevertheless, in fiber-based photon pair sources, an important source of noise is constituted by background photons generated by spontaneous Raman scattering of the pump mode (which occurs within a spectral window of ~ 50 THz [11] towards the red from the pump frequency). We have shown in Ref. 7 that fiber bi-refringence together with cross-polarized SFWM can result in factorable states in a geometry such that signal/idler separation from the pump exceeds the pump Raman bandwidth. In the current paper, we further explore the use of non-birferingent fiber for factorable photon-pair generation. We show that it is likewise possible to find non-birefringent fiber geometries which permit the generation of both symmetric and asymmetric factorable photon pairs in the visible and/or near-infrared, with sufficient spectral separation from the pump so as to avoid Raman contamination while retaining a relatively modest overall span of pump and generation frequencies, through degenerate-pumps, co-polarized SFWM.

Evidently, a crucial consideration in the design of photon-pair sources is the attainable emission flux, or alternatively the attainable conversion efficiency. In Ref. 12 we have presented expressions of the SFWM conversion efficiency valid for both the monochromatic-pumps and pulsed-pumps regimes, as well as for both the degenerate-pumps and non-degenerate-pumps configurations. We have studied the dependence of the conversion efficiency on various key experimental parameters. In this paper, we present a comparison of the SFWM conversion efficiency involving outer-loop phasematching, for which the signal and idler modes are considerably removed from the pump (*e.g.* hundreds of nm), and inner-loop phasematching for which the signal and idler modes can be comparatively in much greater spectral proximity to the pump. Note that we present a precise definition of what is meant by inner-loop and outer-loop phasematching in Sec. 3.

2. Spontaneous four-wave mixing theory

In this paper we study the spontaneous four-wave mixing process in a single-mode optical fiber with a third-order nonlinear susceptibility $\chi^{(3)}$. In this process, two photons from pump fields E_1 and E_2 are jointly annihilated to create a photon pair comprised of one photon in the signal mode, $\hat{E}_s$, and one photon in the idler mode $\hat{E}_i$. For the analysis which we present here, we concentrate on SFWM sources for which all four participating fields are co-polarized and propagate in the fundamental mode of the fiber (HE_{11}). Likewise, we concentrate on SFWM sources based on photonic crystal fiber, which offers a greater scope for photon-pair state engineering [7]. In this process, for a fiber exhibiting two zero dispersion frequencies, and for a given pump frequency, phasematching tends to be fulfilled for two distinct sets of signal and idler frequencies. The purpose of this paper is on the one hand to explore the photon-state engineering potential of "inner-loop" phasematching, *i.e.* for the phasematched signal and idler solutions closest to the pump frequency. On the other hand, we compare "inner-loop" and "outer-loop" photon pairs in terms of the attainable conversion efficiency.

The two-photon state produced by SFWM in an optical fiber of length L can be shown to be given by [7]:

$$|\Psi\rangle = |0\rangle_s|0\rangle_i + \kappa \int d\omega_s \int d\omega_i F(\omega_s,\omega_i) |\omega_s\rangle_s |\omega_i\rangle_i . \quad (1)$$

Here, $F(\omega_s,\omega_i)$ is the joint spectral amplitude function (JSA), which describes the spectral entanglement properties of the generated photon pair; it is given by [7]:

$$F(\omega_s,\omega_i) = \int d\omega\, \alpha(\omega)\alpha(\omega_s+\omega_i-\omega) \times \mathrm{sinc}\left[\frac{L}{2}\Delta k(\omega,\omega_s,\omega_i)\right] e^{i\frac{L}{2}\Delta k(\omega,\omega_s,\omega_i)}. \quad (2)$$

The JSA is given, for degenerate pumps, in terms of the pump spectral amplitude function $\alpha(\omega)$, and the phasemismatch function $\Delta k(\omega,\omega_s,\omega_i)$, that in the case where the two pumps, signal and idler are co-polarized, is given by

$$\Delta k(\omega,\omega_s,\omega_i) = k(\omega) + k(\omega_s+\omega_i-\omega) - k(\omega_s) - k(\omega_i) - 2\gamma_p P, \quad (3)$$

which includes a self/cross-phase modulation contribution for the pump with peak power P, characterized by the nonlinear parameter γ_p [13]. The energy conservation constraint is apparent in the argument of the second term of the phase mismatch [see Eq. (3)].

Modeling $\alpha(\omega)$ as a Gaussian function with bandwidth σ and central frequency ω_p^o, so that

$$\alpha(\omega) = \frac{2^{1/4}}{\pi^{1/4}\sqrt{\sigma}} \exp\left[-\frac{(\omega-\omega_p^o)^2}{\sigma^2}\right], \quad (4)$$

the constant κ in Eq. (1), which is related to the generation efficiency, is given by

$$\kappa = i\frac{2(2\pi)^{1/2}\epsilon_o c n_p}{\hbar\omega_p^o}\frac{L\gamma P}{\sigma}. \quad (5)$$

In Eq. 5, ϵ_o is the vacuum electrical permittivity, $\hbar$ is Planck's constant, c is the speed of light in vacuum, $n_p \equiv n(\omega_p^o)$ is the refractive index, P is the peak pump power, and the parameter γ is the nonlinear coefficient that results from the interaction of the four participating fields in the SFWM process. This parameter determines in part the amplitude κ of the two-photon component of the state (which in turn defines the conversion efficiency) and is given by

$$\gamma = \frac{3\chi^{(3)}\omega_p^o}{4\epsilon_o c^2 n_p^2 A_{eff}}, \quad (6)$$

where A_{eff} is the effective interaction area among the four fields given by

$$A_{eff} = \frac{1}{\int dx \int dy A_p(x,y)^2 A_s^*(x,y) A_i^*(x,y)}. \quad (7)$$

In the expression for the effective area [see Eq. (7)], functions $A_\mu(x,y)$ (with $\mu = p,s,i$) represent the transverse field distributions for each of the four participating fields, evaluated at frequency ω_μ°, and are assumed to be normalized so that

$$\int\int dxdy |A_\mu(x,y)|^2 = 1.$$

Note that, in general, γ is different from γ_p of Eq. (3) [12].

By making use of Eq. (4) and a linear approximation for the phasemismatch, it is possible to obtain an expression for the joint spectral amplitude in closed analytic form. Expanding $k(\omega_\mu)$ in a first-order Taylor series around frequencies ω_μ^o for which perfect phase-matching is attained (where $\mu = 1,2,s,i$), and defining the detunings $\nu_s = \omega_s - \omega_s^o$

and $\nu_i = \omega_i - \omega_i^o$, the approximate phasemismatch Δk_{lin} is given, for degenerate pumps, by

$$L\Delta k_{lin} = L\Delta k^{(0)} + T_s\nu_s + T_i\nu_i,$$

where $\Delta k^{(0)}$, given by Eq. (3) and evaluated at the frequencies ω_μ^o, must vanish to guarantee phase-matching at these central frequencies. The coefficients T_μ represent the group-velocity mismatch between the pump centered at frequency ω_p^o and each of the generated photons centered at the frequency ω_μ^o. They are given by

$$T_\mu = L\left[k_p^{(1)}\left(\omega_p^o\right) - k_\mu^{(1)}\left(\omega_\mu^o\right)\right], \tag{8}$$

where the superscript $^{(1)}$ denotes a frequency derivative. Note that this approach requires *a priori* knowledge, for given pump fields, of the signal and idler frequencies [ω_s^o and ω_i^o] at which perfect phase-matching is achieved. These frequencies can be determined by solving (for example numerically) the condition $\Delta k^{(0)} = 0$ [see Eq. (3)], which requires knowledge of the dispersive characteristics of the fiber. It can be shown that within the linear approximation, the integral in Eq. (2) can be carried out analytically, yielding

$$F_{lin}\left(\nu_s, \nu_i\right) = \alpha\left(\nu_s, \nu_i\right)\phi\left(\nu_s, \nu_i\right), \tag{9}$$

where $\alpha\left(\nu_s, \nu_i\right)$ is the pump envelope function and $\phi\left(\nu_s, \nu_i\right)$ describes the phase-matching properties of the fiber. For degenerate pumps these functions are given by

$$\alpha\left(\nu_s, \nu_i\right) = \exp\left[-\frac{\left(\nu_s + \nu_i\right)^2}{2\sigma^2}\right], \tag{10}$$

$$\phi\left(\nu_s, \nu_i\right) = \mathrm{sinc}\left[\frac{L\Delta k_{lin}}{2}\right]\exp\left[i\frac{L\Delta k_{lin}}{2}\right]. \tag{11}$$

1. Conversion efficiency for the SFWM process

An important aspect to be considered in designing a photon-pair source is the source brightness. Recently, we have derived expressions for the SFWM conversion efficiency for different pump configurations [12]. By replacing Eqs. (2), (4), and (5) in Eq. (1), we have shown that the conversion efficiency for the pulsed-pump regime can be written as

$$\eta = \frac{2^7\hbar c^2 n_p^2}{(2\pi)^3 R}\frac{L^2\gamma^2 p}{\sigma^2\omega_p^o} \times \int d\omega_s \int d\omega_i h(\omega_s, \omega_i)\left|f(\omega_s, \omega_i)\right|^2, \tag{12}$$

in terms of a version of the joint spectral amplitude [see Eq. (2)] defined as $f(\omega_s, \omega_i) = \sigma(\pi/2)^{1/2}F(\omega_s, \omega_i)$, which does not contain factors in front of the exponential and sinc functions so that all pre-factors appear explicitly in Eq. (12). Here, the function $h(\omega_s, \omega_i)$ is given by

$$h(\omega_s, \omega_i) = \frac{k_s^{(1)}\omega_s}{n_s^2}\frac{k_i^{(1)}\omega_i}{n_i^2}, \tag{13}$$

where $k_\mu^{(1)} \equiv k^{(1)}(\omega_\mu)$ represents the first frequency derivative of $k(\omega)$, and $n_\mu \equiv n(\omega_\mu)$.

In Eq. (12), p is the average pump power, and R is the pump repetition rate. For a pump with a Gaussian spectral envelope, p and R are related to the peak power P through the relation $P = p\sigma/(\sqrt{2\pi}R)$. Note that the conversion efficiency [Eq. (12)] which we report here has been calculated in the spontaneous limit, where the probability of multiple-pair emission is neglected.

In the present paper, we show results of the conversion efficiency for specific SFWM-source designs. On the other hand, we describe conditions which permit the generation of the important class of factorable states, which are defined so that $F\left(\omega_s, \omega_i\right)$ can be expressed as the product of two functions, $F\left(\omega_s, \omega_i\right) = S(\omega_s)I(\omega_i)$, where the functions $S(\omega)$ and $I(\omega)$ depend only on the signal and idler frequencies, respectively. On the other hand, we show that configurations based on inner-loop phasematching may used for the generation of photon pairs with an arbitrary degree of spectral correlations. For a more complete discussion of SFWM theory, see Refs. 7 and 12.

3. Phase and group-velocity matching properties of photonic crystal fibers

The SFWM phasematching properties are determined by the frequency-dependence of the propagation constant $k(\omega)$. We adopt the step-index model of Ref. 14, which permits a rough estimate of the frequency-dependence of the propagation constant $k(\omega)$ exhibited by a photonic crystal fiber (PCF), by modeling the discontinuous cladding as an effective continuous medium. This allows a straightforward exploration of the spectral entanglement properties of the resulting photon pairs in $\{r, f\}$ parameter space, where r is the core radius and f the air-filling fraction of the PCF cladding. In order to design a two-photon source to be used in an experiment, knowledge of the exact fiber dispersion is required for a full quantitative prediction of the generated frequencies and the type/degree of signal-idler spectral correlations, expected for a given fiber and for a given pump mode. If the transverse geometry is known, and assuming no longitudinal variations of this geometry along the fiber, sophisticated numerical methods may be used for calculating the expected dispersion relation [15]. In this paper, which relies on an approximate dispersion relation, we aim to explore the full range of two-photon states which can be obtained utilizing inner-branch phasematching, rather than to obtain a precise quantitative prediction of photon pair properties for a given experimental situation.

A plot of the perfect phasematching contour [$\Delta k(\omega_p, \omega_s, 2\omega_p - \omega_s) = 0$] in the space formed by the generated and pump frequencies, gives for each pump frequency the expected signal and idler central frequencies ω_s^o and ω_i^o. Such a perfect phasematching contour is illustrated in Fig. 1(a) for a specific PCF with $r = 0.573\,\mu$m and f=0.5,

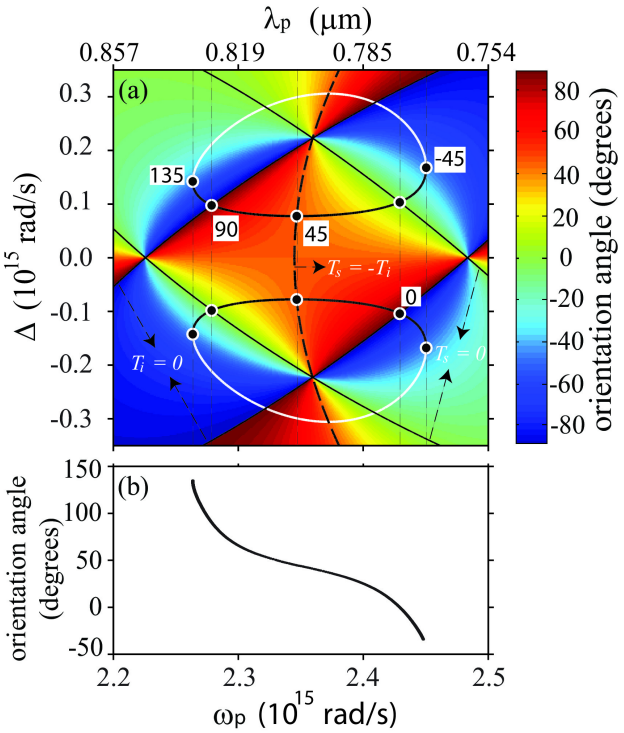

FIGURE 1. (a) Black, solid curve: phase-matching ($\Delta k = 0$) contour for SFWM in the degenerate pump case. Colored background: phase-matching orientation angle. Black, dashed lines: symmetric group velocity matching (GVM) contour ($T_s = -T_i$). Black, thin lines: asymmetric group velocity matching contour ($T_s = 0$), and asymmetric group velocity matching contour ($T_i = 0$). Along the inner branch of the phase-matching contour we have indicated particular orientation angles of interest. (b) Orientation angle θ_{si}, along the inner loop, plotted as a function of the pump frequency.

pumped by a peak power 50 W, and with $\gamma_p = 70\text{km}^{-1}\text{W}^{-1}$, where the generated frequencies are expressed as detunings from the pump frequency as $\Delta_{s,i} = \omega_{s,i} - \omega_p$; note that energy conservation dictates that $\Delta_s = -\Delta_i \equiv \Delta$. For Fig. 1(a), we have relied on the step-index model, but have considered dispersion to all orders (*i.e.* we have not resorted to the linear approximation of the phasemismatch). The phase-matching contours take the form of two closed loops, as indicated in Fig. 1(a); while one of these loops occurs for $\Delta > 0$, the other loop occurs for $\Delta < 0$. We refer to the inner portion of each of the two loops, shown graphically in Fig. 1(a) by a continuous black line, as the inner loop. Likewise, we refer to the outer portion of the two loops, shown graphically in Fig. 1(a) by a white line, as the outer loop.

Note that while the inner loop is in relative close spectral proximity to the pump, the outer loop can be hundreds of nanometers from the pump wavelength. In this paper we exploit the observation that for certain fiber parameters, the inner-loop signal/idler frequencies (resulting from the power-dependent nonlinear contribution to the phasemismatch Δk) can be separated from the pump, by more than its Raman bandwidth ($\sim$ 50 THz), even for modest pump powers. In this manner, contamination of inner-loop signal and idler modes by background photons generated through spontaneous Raman scattering, which would seriously hamper the usefulness of a photon-pair source based on these modes, can be avoided. For this specific fiber geometry, a continuous pump wavelength range of approximately 103 nm exists, in which parametric generation can be observed, roughly contained by the two zero dispersion wavelengths (ZDWs) ($\lambda_{zd1} = 0.7589$ μm and $\lambda_{zd2} = 0.8468$ μm).

From Eq. (10) it is clear that the pump envelope function exhibits contours of equal amplitude in $\{\omega_s, \omega_i\}$ space with negative unit slope. In contrast, the contours of the phase-matching function $\phi(\omega_s, \omega_i)$ are characterized by a slope in $\{\omega_s, \omega_i\}$ space given by $\theta_{si} = -\arctan(T_s/T_i)$ [with T_μ given according to Eq. (8)]. The colored background in Fig. 1 indicates the slope of the phase-matching contour, or orientation angle in $\{\omega_s, \omega_i\}$ space, ranging from $\theta_{si} = -90°$ in blue to $\theta_{si} = +90°$ in red.

The type of spectral correlations observed in a SFWM two-photon state is determined in part by the slope $\theta_{\Delta p}$ of the perfect phasematching contour, related to the orientation angle θ_{si} by $\theta_{\Delta p} = 45° - \theta_{si}$. This relationship implies that if the perfect phasematching contour is in the form of closed loops (which is true for fibers with two zero dispersion frequencies), all orientation angles θ_{si} are possible, controlled by the pump frequency. In this paper we are particularly interested in the inner portion of the phasematching loops. In Fig. 1 we have indicated for a few points along the inner loop, the resulting orientation angle θ_{si}. The full trend of the resulting θ_{si} value along the inner loop may be appreciated in Fig. 1(b), which makes it clear that all possible values of θ_{si} may be reached as one varies the pump frequency. This has the important implication that two-photon states with arbitrary degrees of spectral correlations may be obtained within the inner loops.

In particular, for certain relative orientations and widths of these two phasematching and pump-envelope functions, it becomes possible to generate factorable two-photon states. It can be shown that a factorable state is possible if

$$T_s T_i \leq 0. \tag{14}$$

Among the states which fulfil Eq. (14), those exhibiting a phasematching angle of $\theta_{si} = 45°$, or $T_s = -T_i$, are of particular interest. For these states, in the degenerate pumps case, a factorable, symmetric state is guaranteed if

$$\frac{\Gamma}{2}\sigma^2 |T_s T_i| = 1, \tag{15}$$

where $\Gamma \approx 0.193$ [7]. The condition in Eq. (14) constrains the group velocities: either $k^{(1)}(\omega_s) < k^{(1)}(\omega_p) < k^{(1)}(\omega_i)$, or $k^{(1)}(\omega_i) < k^{(1)}(\omega_p) < k^{(1)}(\omega_s)$ must be satisfied. The condition in Eq. (15) constrains the fiber length and pump bandwidth. Eq. (14) implies that the region in $\{\Delta, \omega_p\}$ space in which factorability is possible is bounded by the loci corresponding to the conditions $T_s = 0$ and $T_i = 0$ (shown in Fig. 1 by solid, thin black lines).

Once the dispersion relation for a given fiber is known, the next step in designing a factorable photon pair source con-

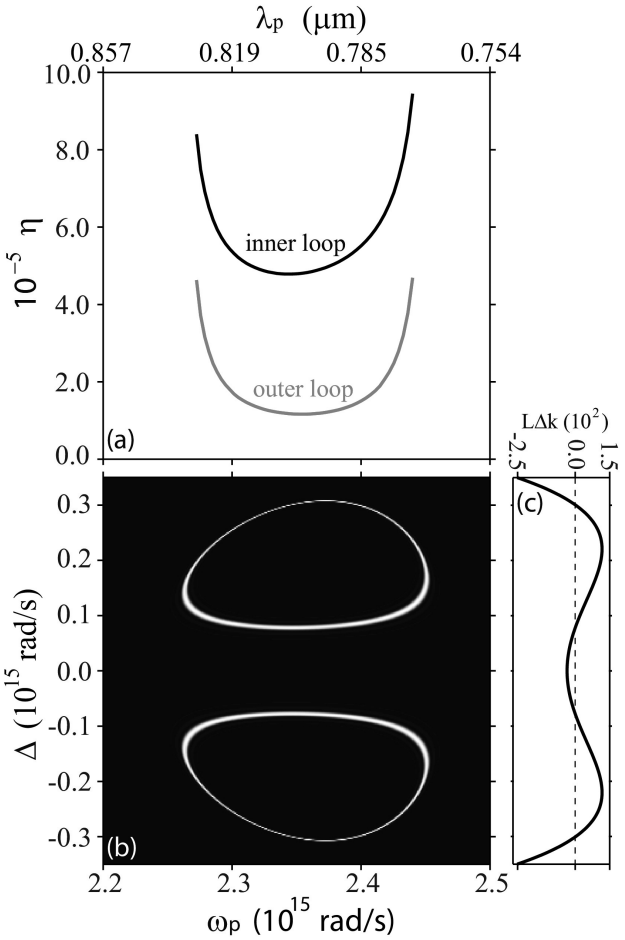

FIGURE 2. (a) Conversion efficiency as a function of pump frequency. The red and black lines correspond to the outer and inner branches of the perfect phasematching contour in Fig. (1), respectively. (b) Signal-mode, single-photon spectrum, for different pump frequencies. (c) $L\Delta k$ as a function of Δ, for a specific value of the pump frequency, $\omega_p = 2.3510^{15}\text{rad}/s$.

sists in identifying the pump wavelengths that satisfy the required group-velocity matching condition, amongst those which also satisfy phase-matching. In particular, symmetric factorable two-photon states, for which the signal and idler photons have identical spectral widths, are possible if $\theta_{si} = 45^\circ$. In this case symmetric group-velocity matching $2k_p^{(1)} = k_s^{(1)} + k_i^{(1)}$ (or equivalently $T_s = -T_i$) is attained, and the phase-matching contours are oriented so that its contours have unit slope. The frequency values that fulfill this condition are represented by a labeled black dashed line (see Fig. 1). The pump frequency that permits symmetric factorable states can be determined from the intersection of the phase-matching contour with the group-velocity matching contour.

Similarly, asymmetric factorable two-photon states, for which the signal and idler spectral widths differ greatly, are possible if $\theta_{si} = 0^\circ$ or $\theta_{si} = 90^\circ$. These special phasematching orientations are possible if an asymmetric group-velocity matching condition is fulfilled, *i.e.* $k_p^{(1)} = k_s^{(1)}$ or $k_p^{(1)} = k_i^{(1)}$ (or equivalently $T_s = 0$ or $T_i = 0$). In this case the phasematching contours are oriented parallel to the ω_s or ω_i axes. In addition, Eq. (15) leads to the condition that $T_i \gg 1/\sigma$ (for $T_s = 0$) or $T_s \gg 1/\sigma$ (for $T_i = 0$).

4. Conversion efficiency as a function of the pump frequency

As we have discussed above, the type of spectral correlations in SFWM photon pairs can be controlled by the pump frequency. Different types of spectral correlations, in turn lead to different levels of conversion efficiency, a dependence which we analyze in the current section. For the analysis presented here, we assume the fiber parameters used in the previous section.

We have previously studied the SFWM conversion efficiency as a function of key experimental parameters such as fiber length, pump power, and pump bandwidth [12]. Likewise, in Ref. 12 we have analyzed the pump-wavelength dependence of the conversion efficiency, but restricted our attention to outer-loop photon pairs. In this paper, we are interested in a comparison of outer- and inner-loop SFWM conversion efficiency. To this end, we have restricted the pump frequency range so as to ensure that the outer-loop signal and idler modes do not spectrally overlap the inner-loop signal and idler modes.

For specific numerical calculations, shown below, we have chosen the following values for the pump parameters: bandwidth $\sigma = 25.1$ GHz (which corresponds to a Fourier-transform-limited temporal duration of 94 ps), average power $p = 500$ mW, and repetition rate 100 MHz. The fiber length considered is $L = 5$ m and we assume a nonlinear coefficient $\gamma = 70\text{km}^{-1}\text{W}^{-1}$. The conversion efficiency is calculated in the pump wavelength range 0.7725-0.8295 μm, and results obtained by numerical evaluation of Eq. (12) are shown in Fig. 2(a). The black line corresponds to the inner-loop conversion efficiency, while the red line corresponds to the outer-loop conversion efficiency. From this figure it is evident that throughout the pump frequency range considered here, inner-loop SFWM tends to involve a greater conversion efficiency, by a factor approaching four in this specific case, when compared to outer-loop SFWM.

In order to understand this behavior, in Fig. 2(b) we plot, for each pump frequency the resulting single-photon spectrum $\langle a^\dagger(\Delta)a(\Delta)\rangle$. From this plot, it is evident that the single-photon spectrum tends to be wider for the inner portion of the phasematching loops, compared to the outer portions of the loops. This disparity in the bandwidth of the inner and outer loops may be understood from Fig. 2(c) where we plot the quantity $L\Delta k$ as a function of Δ for a specific value of the pump frequency, $\omega_p = 2.3510^{15}$ rad/s. It may be observed that the slope of $L\Delta k$ vs Δ is much greater for the outer solutions to $L\Delta k = 0$ (outer loop) than for the inner solutions to $L\Delta k = 0$ (inner loop). This implies that the SFWM process is nearly phasematched over a greater spectral width for the inner loop than for the outer loop. The re-

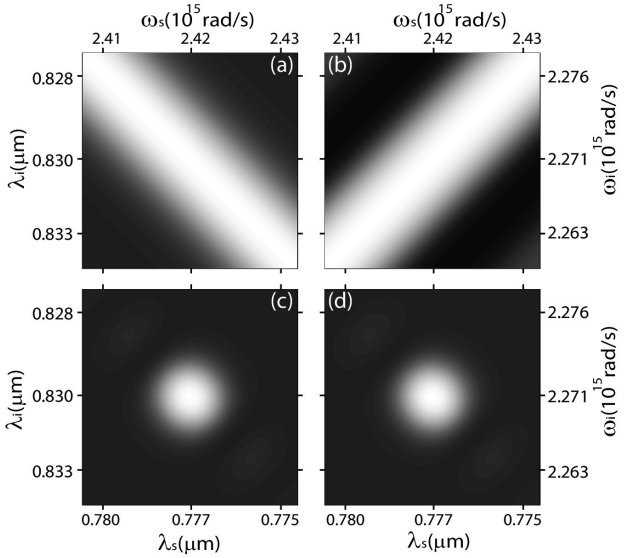

FIGURE 3. Joint spectral intensity (JSI) obtained for the fiber geometry assumed for Fig. 1 ($r = 0.573$ μm and $f = 0.5$) where the pump central wavelength ($\lambda_p^o = 0.803$ μm) is obtained by imposing simultaneous phasematching and group-velocity matching. We consider a pump bandwidth of 1.306 nm and a fiber length of 10 m. The function values are normalized such that white $= 1$ and black =0. (a) Pump envelope function $\alpha(\omega_s, \omega_i)$. (b) Phase-matching function $\phi\,(\nu_s, \nu_i)$. (c) Analytic JSI, obtained from Eq. (9). (d) JSI obtained by numerical integration of Eq. (2).

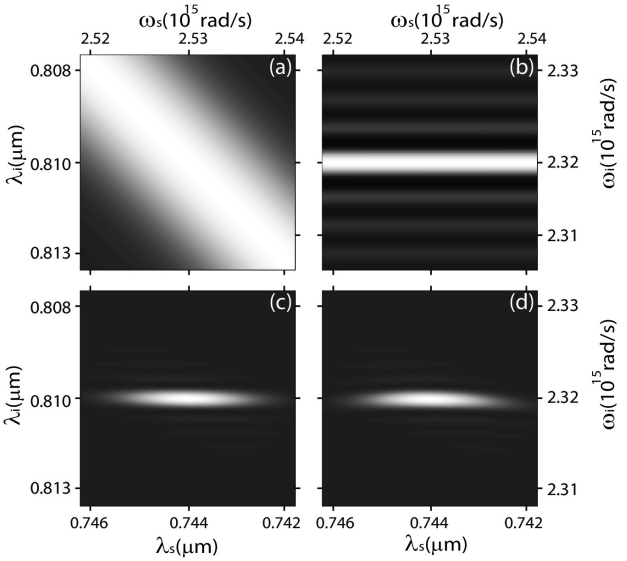

FIGURE 4. Joint spectral intensity (JSI) obtained for the fiber geometry assumed for Fig. 1 ($r = 0.573$ μm and $f = 0.5$) where the pump central wavelength ($\lambda_p^o = 0.7759$ μm) is obtained by imposing simultaneous phasematching and asymmetric group-velocity matching. We consider a pump bandwidth of 1.5 nm and a fiber length of 50 m. The function values are normalized such that white $= 1$ and black $= 0$. (a) Pump envelope function $\alpha(\omega_s, \omega_i)$. (b) Phase-matching function $\phi\,(\nu_s, \nu_i)$. (c) Analytic JSI, obtained from Eq. (9). (d) JSI obtained by numerical integration of Eq. (2).

sulting greater emission bandwidth for the inner loop is the reason for the observed greater conversion efficiency. This points to a potentially important advantage for inner-loop SFWM photon-pair sources: the possibility of obtaining a greater emission flux. In addition, inner-loop SFWM leads to other advantages, such as a narrower overall span of optical frequencies including the pump, signal and idler modes, which can favor simpler experimental setups.

Note that while inner-loop SFWM leads to greater conversion efficiency than outer-loop SFWM, as illustrated in Fig. 2(a), the conversion efficiency vs pump frequency trend is very similar for the two cases. It can be seen that in both cases, the conversion efficiency remains approximately constant in the central portion of the spectral range considered, and climbs towards the edges of this range. In order to understand this behavior, recall that the phasematching orientation angle is controlled by the pump frequency. From Figs. 1 and 2 it can be appreciated that anti-correlated two-photon states, characterized by $\theta_{si} = -45°$, lead to a larger conversion efficiency as compared to other orientations in $\{\omega_s, \omega_i\}$ space. In particular, an orientation of $\theta_{si} = 45°$ tends to minimize the conversion efficiency, and there is a smooth variation of the conversion efficiency between $\theta_{si} = -45°$ and $\theta_{si} = 45°$. The physical reason for this behavior is that for $\theta_{si} = -45°$, the phasematching function overlaps the pump envelope function over a wider spectral range, leading to a greater generation bandwidth [see Fig. 2(b)] which tends to enhance the value of the integral in Eq. (12). Thus, for each of the two types of source, *i.e.* based on outer-loop and inner-loop phasematching, the emission bandwidth tends to increase towards the edges of the pump frequency range considered, tending to also enhance the conversion efficiency.

As we mentioned above, in this paper we are interested in factorable photon-pair sources. Both symmetric and asymmetric GVM are possible using a number of different configurations. For a particular fiber, factorable states can be obtained in both the inner and outer branches of the perfect phasematching contour. In the following sections we provide examples of factorable photon-pair sources based on inner-loop phasematching.

5. Symmetric factorable states

The synthesis of a symmetric, factorable SFWM photon-pair state based on inner-loop phasematching is illustrated in Fig. 3 for the same fiber parameters assumed in Secs. 3 and 4. Figure 3(a) shows the pump envelope function, for a single pump centered at 803 nm with a relatively narrow bandwidth of 1.3 nm. Figure 3(b) shows the phasematching function assuming a fiber length of 10m, while Fig. 3(c) shows the joint spectral intensity $|F_{lin}(\omega_s, \omega_i)|^2$, exhibiting an essentially factorable character. The signal and idler photons are centered at 777.5 nm and 830.7 nm, respectively, so that they are separated from the pump by 77.4 THz. For comparison, Fig. 3(d) shows the joint spectral intensity obtained by numerical integration of Eq. (2) using the full fiber dispersion, revealing that in this case the linear approximation of the

phasematching condition is in fact an excellent approximation. This source leads to a numerically-obtained state purity [defined as $\mathrm{Tr}[\hat{\rho}_s^2]$, where $\hat{\rho}_s$ is the reduced density operator for the signal state] of 0.8754. In fact, the departure from ideal purity is mainly due to sidelobes (related to the sinc function) displaced from the central portion of joint spectral intensity shown in Figs. 3(c) and (d). The purity can be increased by filtering out these sidelobes, which in general contain a small fraction of the total flux. Specifically, for the example shown in Fig. 3, two separate narrowband rectangular-profile spectral filters for the signal and idler modes with equal frequency bandwidth of 10×10^{12} rad s^{-1} increases the purity to 0.9756, while reducing the flux by $\lesssim 6\%$. In this example we have chosen the pump so that it is compatible with, say, a Ti:sapphire laser. Both signal and idler photons can be detected efficiently with a silicon-based avalanche photodiode.

6. Asymmetric factorable states

As indicated in Fig. 1, the fiber parameters assumed in the previous section for symmetric, factorable photon pair generation can also yield asymmetric, factorable photon pairs with $\theta_{si} = 0^\circ$ and $\theta_{si} = 90^\circ$ based on inner-loop phasematching. In particular, a "horizontally"-oriented phasematching function ($\theta_{si} = 0^\circ$) is possible for a pump centered at 775.9 nm. In this case, the group velocity of the signal photon matches the group velocity of the pump and its resulting spectral bandwidth is much larger than the resulting bandwidth of the idler photons. The synthesis of such a state is illustrated in Fig. 4. Figure 4(a) shows the pump envelope function, for a degenerate pump with a relatively narrow bandwidth of 1.5 nm. Figure 4(b) shows the phasematching function assuming a fiber length of 50 m, while Fig. 4(c) shows the joint spectral intensity (JSI) $|F_{lin}(\omega_s,\omega_i)|^2$. The signal and idler photons are centered now at 744.2 nm and 810.5 nm, respectively, so that they are separated from the pump by 103.56 THz. For comparison, Fig. 4(d) shows the joint spectral intensity obtained by numerical integration of Eq. (2). Note that a slight curvature is apparent in the contours of the JSI, resulting from higher dispersion orders. Nevertheless, the structure of the state exhibits an essentially factorable character with a numerically-calculated single-photon purity of 0.945. As in the previous case, the pump is compatible with a Ti:sapphire laser and the generated photons lie in visible / near-infrared region of the spectrum beyond the main spontaneous Raman band. Similarly, for the same fiber, a "vertically"-oriented asymmetric factorable state oriented (parallel to ω_i axes), for which $\theta_{si} = 90^\circ$ or $T_i = 0$, becomes possible for a pump centered at 827 nm (see Fig. 1), obtaining parametric signals centered at 793.06 nm and 864.27 nm, separated from the pump by 97.9 THz.

7. Conclusions

We have studied theoretically photon pair sources based on the process of spontaneous four-wave mixing in photonic crystal fibers. When plotting the generated frequencies vs the pump frequency there are often two phasematched branches, referred to as inner-loop and outer-loop in accordance to the spectral proximity to the pump. In this paper, we have focused on photon-pair sources based on inner-loop phasematching. We have shown that arbitrary spectral correlations in the resulting photon pairs are possible within the inner phasematching loops, as controlled by the pump frequency. In particular, we have shown that if certain group-velocity matching conditions are satisfied, in addition to standard phasematching, both symmetric and asymmetric factorable states are possible. We have shown that fiber designs exist for which the spectral separation between the emission modes and the pump is greater than the width of the spontaneous Raman scattering window, even for modest pump powers, so that the signal and idler modes may be free from Raman contamination. We have compared the SFWM conversion efficiency for the cases of outer- and inner-loop phasematching, and we have found that inner-loop SFWM tends to be brighter than outer-loop SFWM. Likewise we found that for both outer- and inner-loop SFWM, the conversion efficiency has a continuous variation with the pump frequency, where the optimum flux occurs for those pump frequencies for which the signal and idler photons are anti-correlated. We hope that this work will be useful in the design of optimized fiber-based photon-pair sources for quantum information processing applications.

Acknowledgements

This work was supported in part by CONACYT, Mexico, by DGAPA, UNAM and by FONCICYT project 94142.

1. P. Kok *et al.*, *Rev. Mod. Phys.* **79** (2007) 135.
2. M.G. Raymer, J. Noh, K. Banaszek and I.A. Walmsley, *Phys. Rev. A* **72** (2005) 023825.
3. J.E. Sharping, M. Fiorentino, A. Coker, P. Kumar, and R.S. Windeler, *Opt. Lett.* **26** (2001) 1048.
4. J. Rarity, J. Fulconis, J. Duligall, W. Wadsworth, and P. St. J. Russell, *Opt. Express* **13** (2005) 534.
5. W.P. Grice, A.B. U'Ren, and I.A. Walmsley, *Phys. Rev. A* **64** (2001) 063815.
6. A.B. U'Ren *et al.*, *Laser Phys.* **15** (2005) 146.
7. K. Garay-Palmett *et al.*, *Opt. Express* **15** (2007) 14870.
8. M. Halder *et al.*, *Opt. Express* **17** (2009) 4670.
9. O. Cohen *et al.*, *Phys. Rev. Lett.* **102** (2009) 123603.

10. C. Söller *et al.*, **Phys. Rev. A 81** (2010) 031801(R).

11. Q. Lin, F. Yaman, and G.P. Agrawal, *Phys. Rev. A* **75** (2007) 023803.

12. K. Garay-Palmett, A.B. U'Ren, and R. Rangel-Rojo, *Phys. Rev. A* **82** (2010) 043809.

13. G.P. Agrawal, *Nonlinear Fiber Optics, 4th Ed.* (Elsevier, 2007).

14. G.K.L. Wong *et al.*, *Opt. Express* **13** (2005) 8662.

15. Z. Zhu and T. Brown, *Opt. Express* **10** (2002) 853.